Functional partitioning of a liquid-like organelle during assembly of axonemal dyneins

Chanjae Lee[1], Rachael M. Cox[1], Ophelia Papoulas[1], Amjad Horani[2], Kevin Drew[1], Caitlin C. Devitt[1], Steven L. Brody[3], Edward M. Marcotte[1]* and John B. Wallingford[1]*

1. Department of Molecular Biosciences, University of Texas, Austin, TX 78712, USA.
2. Department of Pediatrics, Washington University School of Medicine, St. Louis, MO 63110, USA.
3. Department of Medicine, Washington University School of Medicine, St. Louis, MO 63110, USA.

*To whom correspondence should be addressed:
Wallingford@austin.utexas.edu or Marcotte@icmb.utexas.edu

Abstract

Ciliary motility is driven by axonemal dyneins that are assembled in the cytoplasm before deployment to cilia. Motile ciliopathy can result from defects in the dyneins themselves or from defects in factors required for their cytoplasmic pre-assembly. Recent work demonstrates that axonemal dyneins, their specific assembly factors, and broadly acting chaperones are concentrated in liquid-like organelles in the cytoplasm called DynAPs. Here, we use *in vivo* imaging to show that inner dynein arm (IDA) and outer dynein arm (ODA) subunits are partitioned into non-overlapping sub-regions within DynAPs. Using affinity purification mass-spectrometry of *in vivo* interaction partners, we also identify novel partners for inner and outer dynein arms. Among these, we identify C16orf71/Daap1 as a novel axonemal dynein regulator. Daap1 interacts with ODA subunits, localizes specifically to the cytoplasm, is enriched in DynAPs, and is required for the deployment of ODAs to axonemes. Our work reveals a new complexity in the structure and function of a cell-type specific liquid-like organelle that is directly relevant to a human genetic disease.

Introduction

Motile cilia are microtubule-based cellular projections and their oriented beating generates fluid flows that are critical for development and homeostasis. Ciliary beating is driven by a complex set of axoneme-specific dynein motors that drive sliding of the axonemal microtubule doublets. Based on their relative positions within the axoneme, these motors are classified as either outer dynein arms (ODAs) or inner dynein arms (IDAs), the former driving ciliary beating generally, and the latter tuning the waveform (Kamiya and Yagi, 2014; King, 2018b). Mutations in genes encoding ODA or IDA subunits are the dominant cause of the motile ciliopathy syndrome known as primary ciliary dyskinesia (PCD; MIM 244400). This genetic disease results in repeated sinopulmonary disease, bronchiectasis, cardiac defects such as heterotaxy, situs anomalies, and infertility (Horani et al., 2016; Mitchison and Valente, 2017). Interestingly, PCD can also result from mutations in genes encoding any of an array of cytoplasmic proteins collectively known as Dynein Axonemal Assembly Factors (DNAAFs)(Desai et al., 2018; Fabczak and Osinka, 2019).

Axonemal dynein motors were known to be pre-assembled in the cytoplasm before deployment to cilia (Fowkes and Mitchell, 1998), but the first description of DNAAFs came later, with the identification of *KTU* (aka *DNAAF2*)(Omran et al., 2008). Studies of motile ciliopathy patients have now defined an array of cytoplasmic DNAAFs that are never part of the axoneme, yet when mutated result in loss of axonemal dyneins, and in turn, defective cilia beating (Diggle et al., 2014; Horani et al., 2012; Horani et al., 2013; Kott et al., 2012; Mitchison et al., 2012; Moore et al., 2013; Olcese et al., 2017; Paff et al., 2017; Tarkar et al., 2013; Zariwala et al., 2013). These specialized DNAAFs are now known to act in concert with ubiquitous, broadly-acting chaperones of the Heat Shock Family (Cho et al., 2018; Li et al., 2017; Mali et al., 2018; Olcese et al., 2017; Omran et al., 2008; Paff et al., 2017; Tarkar et al., 2013; Yamaguchi et al., 2018; Yamamoto et al., 2010; Zhao et al., 2013; Zur Lage et al., 2018).

How DNAAFs organize the assembly of axonemal dyneins is a complex question, as each axoneme contains an array of closely related multiprotein complexes (King, 2018a). For example, ODAs and IDAs incorporate diverse heavy, intermediate, and light chains encoded by distinct genes; few subunits are shared. Moreover, at least eight distinct IDA sub-types and two ODA sub-types have been described (Dougherty et al., 2016; Fliegauf et al., 2005; King,

2018a). Generally, disruption of any single DNAAF has been found to impact both ODAs and IDAs (Fabczak and Osinka, 2019), but a recent study suggests that distinct DNAAFs may be dedicated for the assembly of specific subsets of dyneins (Yamaguchi et al., 2018). Another recent study has suggested that distinct DNAAFs may catalyze specific stages of the dynein assembly process (Mali et al., 2018). This complexity motivates another key question, this one regarding the spatial organization of axonemal dynein assembly.

Several studies indicated that the DNAAFs and chaperones act together in cytosolic foci (Diggle et al., 2014; Horani et al., 2012; Li et al., 2017; Mali et al., 2018), and we recently demonstrated that DNAAFs, chaperones, and axonemal dynein subunits are sequestered in specialized membrane-less organelles that we termed DynAPs (Huizar et al., 2018). DynAPs are multiciliated cell-specific organelles that display hallmarks of biological phase separation, with DNAAFs and chaperones fluxing through rapidly while dynein subunits are stably retained (Huizar et al., 2018). Though DynAPs display properties similar to many ubiquitous liquid-like organelles (Banani et al., 2017; Shin and Brangwynne, 2017), little else is known of the cell biology underlying DynAP assembly or function.

We show here that DynAPs contain functionally distinct sub-compartments. Confocal imaging revealed that the organelles defined by enrichment of DNAAFs and/or chaperones are sub-divided into sub-compartments specifically enriched for ODA or IDA subunits. Affinity-purification and mass-spectrometry of IDA and ODA subunits from MCCs identified several novel interactors, including the uncharacterized protein Daap1/C16orf71. We show that Daap1 is a cytoplasmic protein that is enriched in DynAPs in both human and *Xenopus* multiciliated cells (MCCs). Moreover, Daap1 localization is restricted to the ODA sub-region of DynAPs, where assays of fluorescence recovery after photobleaching (FRAP) show it is stably retained. Finally, disruption of Daap1 elicits a severe loss of ODAs from motile cilia. These data provide new insights into the structure and function of a still poorly defined, cell-type specific, disease-associated organelle.

Results:

Dynein arm subunits occupy sub-regions within DynAPs

The *Xenopus* embryo epidermis is a mucociliary epithelium that serves as a highly tractable model for understanding motile cilia (Hayes et al., 2007; Walentek and Quigley, 2017; Werner and Mitchell, 2011). Using this system, we previously showed that while DNAAFs, chaperones, and dyneins all co-localize in DynAPs with the canonical DNAAF, Ktu/Dnaaf2, dynein subunits displayed relatively more variable co-localization (Huizar et al., 2018). Here, we explored these localization patterns in more detail by pairwise co-expression of an array of fluorescently tagged DNAAFs, Hsp chaperones, and axonemal dynein subunits. We examined their localization in *en face* optical sections through the cytoplasm of *Xenopus* MCCs *in vivo* using confocal microscopy (Fig. 1A).

We found, for example, that the Hsp co-chaperone Stip1/Hop displayed essentially total co-localization with the assembly factor Dnaaf5/Heatr2 (Fig. 1B), while by contrast, the outer dynein arm subunit Dnai2 clearly displayed only partial overlap with Dnaaf5 (Fig. 1C). In fact, pairwise tests of five distinct DNAAFs and three chaperones revealed consistent, near total co-localization in all combinations (Fig. 1D, E). Conversely, pairwise tests with three different axonemal dynein subunits consistently revealed only partial co-localization (Fig. 1F). In all

cases, IDA or ODA subunits occupied distinct, well-demarcated sub-regions within DNAAF- or chaperone-labelled DynAPs.

Inner and outer arm dyneins are partitioned to distinct sub-compartments

We then performed pairwise tests of co-localization of several axonemal dynein subunits. Strikingly, we found that IDAs and ODAs were partitioned into mutually exclusive sub-regions within DynAPs. For example, the ODA subunit Dnai2 displayed complete co-localization with two additional ODA sub-units, Dnai1 and Dnal4 (Fig. 2A, B). By contrast, Dnai2 displayed very little colocalization with IDA-*f* subunit Wdr78 or the IDA-*a, c, d* subunit Dnali1 (Fig. 2C, D). Together, these data suggest that axonemal dynein subunits are partitioned into functionally distinct sub-regions; based upon their contents, we will refer to these here as “ODA sub-DynAPs” and “IDA sub-DynAPs.”

Affinity purification and mass-spectrometry identifies specific *in vivo* interactors for vertebrate inner and outer dynein arm subunits in *Xenopus* multiciliated cells

Given the essential role of cytoplasmic DNAAFs and chaperones in assembly of axonemal dyneins (Desai et al., 2018; Fabczak and Osinka, 2019), we reasoned that sub-DynAPs may also contain regulatory factors with specific roles in the assembly or deployment of either IDAs or ODAs. To test this idea, we sought to determine the interactomes of IDAs and ODAs directly in MCCs. We therefore developed a method to perform affinity purification and mass-spectrometry (APMS) of *in vivo* interaction partners using *Xenopus* mucociliary epithelium and then examined the localization of interaction partners using *in vivo* imaging.

For this experiment, we took advantage of organotypically cultured explants of pluripotent ectoderm from early *Xenopus* embryos (so-called “animal caps”), which can be differentiated into a wide array of organs and tissues, including mucociliary epithelium (Ariizumi et al., 2009; Walentek and Quigley, 2017; Werner and Mitchell, 2012). We and others have used such explants previously for large-scale genomic studies of ciliogenesis and cilia function (Chung et al., 2014; Kim et al., 2018; Ma et al., 2014; Quigley and Kintner, 2017; Walentek et al., 2016).

As baits for APMS, we used GFP-fusions to either IDA or ODA subunits, expressing them specifically in MCCs using a well-defined MCC-specific α-tubulin promoter (Deblandre et al., 1999; Tu et al., 2018). For each experiment, we excised ~750 animal caps and cultured them until MCCs developed beating cilia (NF stage 23)(Fig. 3A, green, blue arrows). Protein was isolated from these tissue explants and APMS was performed using an anti-GFP antibody (Fig. 3A). To control for non-specific interactions, each experiment was accompanied by a parallel APMS experiment using un-fused GFP (Fig. 3A, gray), the results of which were then used to subtract background (Fig. 3A, right; see Methods) by calculating a Z-test and fold change for differential enrichment for each protein (see Methods, Supp. Fig. 1). To identify ODA interactors, we used Dnai2-GFP; for IDAs we used Wdr78-GFP (King, 2018b).

For both Dnai2-GFP and Wdr78-GFP, we found that the bait itself was the most strongly enriched protein, providing an important positive control (Supp. Tables 1, 2). Dnai2 pulldown strongly enriched for known ODA-specific sub-units, including the intermediate chain Dnai1, the light chain Tctex1d1, as well as the heavy chain Dnah9 (Fig. 3B, Supp. Fig. 1A; Supp. Table 1). Conversely, our Wdr78 sample was enriched for IDA components, specifically the IDA-*f* subtype, as expected (Fig. 3C). These included the axonemal dynein heavy chains Dnah2 and Dnah10, as well as several light and intermediate chains (Fig. 3C; Supp. Fig. 1A; Supp. Table

2). APMS for both Dnai2 and Wdr78 also identified subunits known to be shared by both ODAs and IDAs, such as Dynll1 and Dynlt1 (Fig. 3B, C).

Our data therefore demonstrate that the compositions of ODAs and *f*-type IDAs in *Xenopus* MCCs are highly similar to those demonstrated in *Chlamydomonas* (see (King, 2018b). There was, however, one key exception, a reciprocal and high-confidence interaction between Dnai2 and Wdr78 (Supp. Tables 1, 2). A similar, though less robust, result was also reported in mouse testes (Zhang et al., 2019), suggesting the possibility that these intermediate subunits may be shared between ODAs and *f*-type IDAs in vertebrate motile cilia.

Finally, we identified weaker but consistent interaction of Dnai2 and Wdr78 with an array of chaperones and assembly factors, including Ruvbl1/2, Spag1, Heatr2/Dnaaf5, and Dnaaf1 (Supp. Tables 1, 2), consistent with findings that these proteins are enriched in DynAPs and are essential for axonemal dynein assembly (Fabczak and Osinka, 2019; Huizar et al., 2018). These data provide new insights into the specific ODA and IDA composition in vertebrate MCCs and also serve as positive controls for the specificity of our APMS approach in MCCs.

Identification and localization of novel IDA and ODA interactors

Importantly, our APMS identified not only known interactors, but also several novel interaction partners. For example, we observed interaction between Dnai2 and Nme9 (Fig. 3B). Nme9 is highly similar to the *Chlamydomonas* ODA light chain LC3 and is present in the axonemes of airway cilia and sperm flagella in mice (Sadek et al., 2003). As in mice, *Xenopus* GFP-Nme9 localized to MCC axonemes (Fig. 4A). More importantly, however, we also observed GFP-Nme9 in the cytoplasm, where it colocalized with Dnai2 specifically in ODA sub-DynAPs (Fig. 4B, C).

Another notable interaction was that between Wdr78 and Wdr18 (Fig. 3C). This result is significant because Wdr18 has been implicated in the control of ciliary beating, but its mechanism of action is entirely unknown (Gao et al., 2011; Silversides et al., 2012). Interestingly, Wdr18-GFP was not present in the axonemes of motile cilia (not shown) but did localize to DynAPs (Fig. 4D). Interestingly, Wdr18-GFP was also strongly enriched in the apical cytoplasm of MCCs, near the basal bodies (Fig. 4E). Similarly, another IDA interactor, Sf3a3 (Fig. 3C), was also absent from axonemes (not shown), but did localize in DynAPs (Fig. 4F). This protein was previously implicated in splicing (Kramer et al., 2005), and we also observed Sf3a3-GFP in nuclear foci in *Xenopus* MCCs (not shown). Together, these data demonstrate that our APMS approach in *Xenopus* effectively identified novel, biologically plausible IDA and ODA interacting proteins *in vivo*.

C16orf71/Daap1 is a novel ODA-interacting protein with an interesting evolutionary trajectory

The most interesting interaction we identified in this study was that between Dnai2 and C16orf71 (Fig. 3B). Though highly conserved among vertebrates, this protein has yet to be the subject of even a single published study. We first sought to confirm that C16orf71 is a *bona fide* ODA interactor using a reciprocal APMS experiment, with GFP-tagged *Xenopus* C16orf71 as the bait. This analysis revealed interaction of C16orf71 not only with Dnai2, but also other ODA subunits such as Dnai1, Dnai2, Dnah9 and Nme9, as well as Ruvbl1 (Fig. 5A; Supp. Fig. 1C, Supp. Table 3). Based on these findings and data described below, we propose to rename this protein Daap1, for Dynein Axonemal-Associated Protein 1.

In situ hybridization revealed that *Xenopus Daap1* expression was enriched in MCCs in the epidermis and the nephrostomes of the pronephros (Fig. 5B). Likewise, examination of data from the Human Protein Atlas (Uhlén et al., 2015) revealed that human Daap1 protein is present exclusively in tissues with motile cilia (Fig. 5C). Interestingly, while Daap1 is conserved among vertebrates, it appears to have followed an interesting evolutionary trajectory. In mammals, including humans, orthologs of Daap1 are composed entirely of a domain of unknown function (DUF4701), which phylogenetic analysis suggests is vertebrate-specific (Fig. 5D). Our analysis of this sequence suggests it is intrinsically disordered (Fig. 5E), a feature commonly associated with liquid-like organelles. By contrast, all non-mammalian vertebrate Daap1 orthologs contain not only the DUF4701 domain, but also a long C-terminal extension harboring, remarkably, an NDK domain similar to those in Nme8 and Nme9 (Fig. 5D). We therefore chose this novel ODA interactor for more in-depth study.

Daap1 is a DynAP-specific protein in *Xenopus* and human MCCs

We next examined the localization of the Daap1 protein in *Xenopus* MCCs. Intriguingly, no signal was detectable in MCC axonemes as marked by Dnai2, and instead, Daap1-GFP was localized exclusively to foci in the cytoplasm of MCCs (Fig. 6A, B). Daap1-GFP strongly co-localized with Dnai2 (Fig. 6B), suggesting that the interaction we identified by APMS occurs in DynAPs. Indeed, Daap1 displayed a partial co-localization with the Dnaaf2 similar to that observed in the cytoplasm for other ODA subunits (Fig. 6C). Finally, Daap1 displayed little or no overlap with Wdr78-GFP (Fig. 6D), suggesting that it localized specifically in ODA sub-DynAPs (Fig. 6D).

Because human Daap1 lacks the C-terminal NDK domain present in the *Xenopus* ortholog (Fig. 5D), we were curious to know if the human ortholog also localizes to DynAPs. We therefore performed immunostaining for Daap1 on sections of human lung. As observed in *Xenopus*, Daap1 was not detectable in the axonemes of human MCCs (Fig. 7A, brackets), and cytoplasmic staining for Daap1 was strongly enriched in DynAPs, as indicated by co-labelling for the ODA subunit DNAI1 (Fig. 7A, arrowheads).

This result then prompted us to examine the localization of a deletion construct comprising the isolated N-terminal DUF4701 domain of *Xenopus* Daap1 (*i.e.*, a *Xenopus* equivalent of human Daap1)(Fig. 7B). We found that GFP-Daap1-Nterm also localized to ODA sub-DynAPs in *Xenopus* MCCs (Fig. 7C-E). Thus, despite their divergent evolutionary trajectories, both *Xenopus* and human Daap1 are DynAP-specific cytoplasmic proteins, and the N-terminal DUF4701 domain is sufficient to direct localization to ODA sub-DynAPs.

Daap1 is stably retained in ODA sub-DynAPs

DynAPs are liquid like organelles, and we previously found using FRAP that both the DNAAFs and broadly acting chaperones flux rapidly through these organelles, while both ODA and IDA subunits are stably retained (Huizar et al., 2018). Because Daap1 does not localize to axonemes in either humans or *Xenopus*, its localization to DynAPs suggests a role in ODA processing or assembly, rather than a direct function in ciliary beating. We therefore expected Daap1 to flux rapidly through DynAPs, similar to other cytoplasmic assembly factors. To our surprise, however, FRAP revealed instead that *Xenopus* Daap1 was retained in DynAPs in a manner that was similar, but not identical, to dynein subunit Dnai2 (Fig. 8). Specifically, Daap1 displayed a somewhat slower initial recovery, but rather than plateauing at around 20 seconds, the signal continued to slowly recover for at least 60 seconds (Fig. 8B).

We were also interested to know if human Daap1 displays similar dynamics, but FRAP assays in human MCCs are very challenging. We therefore examined the FRAP kinetics of *Xenopus* Daap1-Nterm as a proxy of the human protein for use in *Xenopus* MCCs. In FRAP assays, Daap1-Nterm displayed essentially identical kinetics to full-length Daap1 (Fig. 8B). This result is consistent with the localization data above and strongly suggests that the DUF4701 domain is sufficient to drive the retention of Daap1 in ODA sub-DynAPs.

Daap1 is required for deployment of ODAs to the axoneme

To date, disruption of all known DNAAF or DynAP-localized chaperones has elicited defects in assembly or deployment of both IDAs and ODAs (Fabczak and Osinka, 2019), consistent with the localization of these proteins throughout the DynAP (Fig. 1). By contrast, our localization and protein interaction data suggest that Daap1 may play a more specific function, specifically in the assembly of ODAs. We tested this idea using morpholino (MO)-mediated knockdown (KD) to disrupt splicing of the *Daap1* transcript in *Xenopus* (Supp. Fig. 2A). Strikingly, Daap1-KD elicited severe loss of ODAs from MCC axonemes (Fig. 9A, B). Both the intermediate chain Dnai2, as well as the light chain Dnal1 were severely reduced, with only small domains of the proximal axoneme labelled by either marker following knockdown (Fig. 9A, B). Importantly, this phenotype was also observed using a second MO targeting a distinct splice site (Supp. Fig. 2B, C).

Given the specific localization of Daap1 to ODA sub-DynAPs, we expected that Daap1 loss should specifically impact axonemal deployment of ODAs, and not IDAs. For the most part, this was indeed the case. We observed little effect of Daap1 loss on the axonemal localization of the IDA-f component Wdr78 or the IDA-*a, c, d* as indicated by Dnali1-GFP (Fig. 9C, D). We confirmed this finding using knockdown and simultaneous double-labelling of ODAs and IDAs with Dnai2-GFP and Wdr78-RFP (Fig. 9E).

Interestingly, however, we did observe modest, but consistent, loss of IDAs specifically from the distal-most portion of MCC axonemes (Fig. 9C, D, inset). In normal MCCs, both ODAs and IDAs are excluded from the distal-most region of the axoneme (Fig. 9C, D, inset), consistent with the known specialization of the distal tips of motile cilia (Soares et al., 2019). We found that Daap1-KD consistently extended this distal IDA-free zone. This result reflects the proximodistally patterned loss of IDAs and ODAs from axonemes observed in zebrafish carrying mutations in PIH-domain containing DNAAFs (Yamaguchi et al., 2018). Thus, Daap1 is a DynAP-specific protein that interacts with ODA subunits and is essential for the deployment of ODAs to axonemes and further suggests a complex interplay of ODAs and IDAs is required to establish the final patterning of motors that drive ciliary beating.

Discussion

Here, we have used live imaging to demonstrate that DynAPs contain sub-compartments that specifically partition inner and outer dynein arm subunits (Fig. 1, 2). Using *in vivo* proteomics, we identify several novel axonemal dynein interactors, including C16orf71/Daap1 (Fig. 3, 5). In both *Xenopus* and humans, Daap1 is present exclusively in the cytoplasm and not in ciliary axonemes. Moreover, the protein is highly enriched in DynAPs, where it is restricted to the ODA sub-DynAP (Fig. 6-8). Remarkably, loss of function experiments revealed a requirement for Daap1 predominantly in the deployment of ODAs throughout the length of MCC cilia, while the impact on IDAs was only very mild, and restricted to only the distal axoneme (Fig. 9). Together, these data are significant for *1)* adding weight to the argument that DynAPs serve a

specific function in the assembly of axonemal dyneins, *2)* demonstrating that sub-DynAPs represent molecularly and functionally distinct spaces within DynAPs, and *3)* suggesting that additional DynAP-specific regulatory factors remain to be discovered.

Novel axonemal dynein interactors

In addition to the mechanistic insights provided by this study (discussed in detail below), our method for APMS and the datasets of *in vivo* IDA and ODA interactors provided here will be a useful resource for future studies. For example, Wdr18 knockdown results in left/right asymmetry defects in zebrafish and mutations in human Wdr18 are associated with congenital heart defects (Gao et al., 2011; Silversides et al., 2012); both phenotypes are indicative of ciliary beating defects, but the mechanism of Wdr18 action is entirely unknown. The data here are significant, then, for connecting Wdr18 to IDAs (Fig. 3D) and for reporting the localization of Wdr18 in motile ciliated cells for the first time. Because we found that Wdr18 was not present in the axonemes of motile cilia but was present in DynAPs and near basal bodies (Fig. 4D, E), our data suggest that Wdr18 function may not relate directly to IDA *function*, but rather to the *assembly* or *transport* of IDAs.

The more curious result here is the interaction of Wdr78 with Sf3a3 (Fig. 3D), a well-defined component of the RNA splicing machinery (Kramer et al., 2005). Though unexpected, this result, and our finding that Sf3a3 is enriched in DynAPs (Fig. 4F) is consistent with our recent report that DynAPs contain both RNA and RNA-associated proteins (Drew et al., 2020), similar to other liquid-like organelles such as stress granules and P bodies (Banani et al., 2017; Lin et al., 2015; Mittag and Parker, 2018). Indeed, we found that Cfap43 and Cfap44, which tether IDA-*f* to microtubules (Fu et al., 2018; Kubo et al., 2018), are both RNA-associated and localized to sub-DynAPs in *Xenopus* MCCs (Drew et al., 2020). Taken together, these findings suggest that the role of RNA-associated proteins in DynAP assembly or function should be a rich area for future investigation.

Daap1 and the Nme family of proteins and ciliary beating

Our data here also shed light on the evolution of motile cilia function and regulation in vertebrates, particularly with respect to Daap1 and the Nme family of NDK proteins (Desvignes et al., 2009). Three Nme proteins have been implicated in motile cilia function, including Nme8, which is orthologous to the LC3 ODA subunit in *Chlamydomonas* and has been implicated in human motile ciliopathy (Duriez et al., 2007; Pazour et al., 2006). Nme5 is also required for ciliary beating in *Xenopus* and mammals, though its mechanism of action remains unknown (Anderegg et al., 2019; Chung et al., 2014; Vogel et al., 2012). Nme9 (aka Txndc6 or Txl-2) is localized to motile cilia in the mouse (Sadek et al., 2003), but its function is also unknown. It is significant, then, that we found Nme9 to be localized to *Xenopus* MCC cilia (Fig. 4A-C). The observed interactions with Dnai2 and Daap1 (Fig. 3) suggest that it too may be an ODA subunit.

Curiously, examination of genome data using Xenbase (Karimi et al., 2018; Session et al., 2016) suggests that *Xenopus* lacks the Nme8 gene, and further exploration in NCBI revealed that many vertebrate genomes contain only Nme8 or Nme9, but not both (not shown). The linkage of an NDK domain to the DUF4701 domain in non-mammalian Daap1 orthologs suggest the possibility that these two protein domains may act in concert, and it is tempting to speculate that the NDK domain of Daap1 in non-mammalian vertebrates may explain the absence of either Nme8 or Nme9 in those genomes, so additional studies in diverse vertebrates will be of interest.

The structure and function of DynAPs

DynAPs have now been observed in human, mouse, *Xenopus* and zebrafish, so it is clear that these organelles represent a conserved element of multiciliated cells (Diggle et al., 2014; Horani et al., 2018; Huizar et al., 2018; Li et al., 2017; Mali et al., 2018). However, the precise function of DynAPs remains unknown, a situation shared with many liquid-like organelles. Genetic evidence suggests that DynAPs are factories for axonemal dynein assembly, as genetic loss of DynAP-localized DNAAFs consistently results in a failure of dynein arm assembly, failure of dynein deployment to axonemes, and defective ciliary beating (Fabczak and Osinka, 2019). Our identification of Daap1 as yet another protein that is enriched in DynAPs and is specifically required for deployment of axonemal dyneins to cilia adds weight to the argument that DynAPs perform a critical assembly or deployment function.

Strictly speaking, however, all DNAAF proteins and chaperones yet studied are present throughout the cytoplasm and *enriched* in DynAPs, so we cannot rule out the possibility that dyneins are normally assembled in the cytoplasm, while DynAPs serve some other function. For example, DynAPs may act in storage or assembly of dyneins for rapid deployment to cilia (e.g. for ciliary regeneration) or for quality control and/or degradation of mis-folded dyneins. Answering such questions is a key challenge, and is one faced generally for liquid-like organelles.

Regardless, our data clearly demonstrate that DynAPs are structurally partitioned, as are many other liquid-like organelles (e.g. (Feric et al., 2016; Jain et al., 2016; Schmidt and Rohatgi, 2016). Moreover, our observation that Daap1 is restricted to ODA sub-DynAPs (Figs. 6, 7) and that its loss results predominantly in ODA defects (Fig. 9) argues that sub-DynAPs reflect a *functional* sub-compartmentalization. Conversely, though it has been suggested that DNAAFs and chaperones act in a relay system to catalyze iterative steps of ODA and IDA assembly (Mali et al., 2018), we found no evidence of physical compartmentalization of any of the tested DNAAFs and chaperones (Fig. 1), suggesting that partitioned localization of those factors is not strictly required. Consistent with this idea, though Ktu has been shown to specifically impact assembly of ODAs and IDA-*c* (Yamaguchi et al., 2018), we found no restriction of Ktu localization within DynAPs (Fig. 1 and see (Huizar et al., 2018)). Together, our findings here provide a deeper cell biological framework in which to understand the complex genetics of dynein assembly in motile ciliated cells.

Acknowledgments

We thank Claire McWhite for consulting and advice on *X. laevis* orthogroup calculations. This work was supported by grants from the NIH (R01 HL117164 and R01 HD085901 to J.B.W.; R01 DK110520, R35 GM122480 to E.M.M.; R01 HL128370 and R01 HL146601 to S.L.B.; NIH K08HL150223 to A.H and K99 HD092613 and LRP to K.D, as well as the Welch Foundation (F-1515) to E.M.M.. Mass spectrometry data collection was supported by CPRIT grant RP110782 to Maria Person and by Army Research Office grant W911NF-12-1-0390.

Materials and Methods

Xenopus embryo manipulations: *Xenopus* embryo manipulations were carried out using standard protocols. Briefly, female adult *Xenopus* were induced to ovulate by injection of hCG (human chorionic gonadotropin). *In vitro* fertilization was carried out by homogenizing a small fraction of a testis in 1X Marc's Modified Ringer's (MMR). Embryos were dejellied in 1/3x MMR with 2.5 %(w/v) cysteine (pH7.8). Embryos were microinjected with mRNA, circular DNA or morpholinos in 2 % Ficoll (w/v) in 1/3x MMR and injected embryos were washed with 1/3x MMR after 2hrs.

Plasmids and MOs for microinjections: *Xenopus* gene sequences were obtained from Xenbase (www.xenbase.org) and open reading frames (ORF) of genes were amplified from the *Xenopus* cDNA library by polymerase chain reaction (PCR), and then are inserted into a pCS10R vector containing a fluorescence tag or Halo tag. In addition to the vectors described previously (Huizar et al., 2018), the following constructs were cloned into pCS vector : ruvbl2-mCherry, mCherry-zmynd10, GFP-wdr78, GFP-dnai1, GFP-dnal4, GFP-dnal1, GFP-nme9, GFP-wdr18, GFP-sf3a3, GFP-c16orf71, GFP-c16orf71 N-term (1-527aa), and Halo-wdr78. These constructs were linearized and the capped mRNAs were synthesized using mMESSAGE mMACHINE SP6 transcription kit (ThermoFisher Scientific). Each 90 pg of each mRNA was injected into two ventral blastomeres. For APMS, GFP-dnai2, GFP-wdr78 and GFP-c16orf71 N-term were inserted into pCS2 vectors under multiciliated-cell specific alpha-tubulin promoter and each 40 pg of each DNA was injected into blastomeres. C16orf71/Daap1 morpholinos were designed to target 1stor 3rdexon-intron splicing junction, The MO sequences and the working concentrations include:
MO #1 : 5'-AGTAAGGTCTGTACACTTACCAGGG-3', 30 ng per injection
MO #2 : 5'-ACAAATGCAAGTTTTTCTTACCTCA-3', 10 ng per injection

Immunoprecipitation of *Xenopus* animal caps for mass-spectrometry: Circular plasmids of GFP only, GFP-dnai2, GFP-wdr78 and GFP-C16orf71 driven by MCC-specific α-tubulin promoter were injected into 4-blastomeres of 4-cell stage *Xenopus* embryos. Approximately 750 Animal caps per sample were isolated at stage 8 using forceps and were cultured in 1X Steinberg's solution (0.58 mM NaCl, 0.64 mM KCl, 0.33 mM $Ca(NO_2)_2$, 0.8 mM $MgSO_4$, 5 mM Tris, 50 µg/ml gentamicin, pH 7.4-7.6) until sibling embryos reached stage 23. The cultured explants were collected and immunoprecipitation (IP) was performed using GFP-Trap Agarose Kit (ChromoTek, cat# gtak-20). Immunoprecipitated proteins were eluted in 2X sample buffer.

Affinity purification-mass spectrometry: Immunoprecipitated proteins were resuspended in SDS-PAGE sample buffer and heated 5 minutes at 95°C before loading onto a 7.5% acrylamide mini-Protean TGX gel (BioRad). After 7 minutes of electrophoresis at 100 V the gel was stained with Imperial Protein stain (Thermo) according to manufacturer's instructions. The protein band was excised, diced to 1 mm cubes and processed by standard trypsin in-gel digest methods for mass spectrometry (for experiments with baits Dnai2 and Wdr78) or by the more rapid method of Goodman *et al.* (Goodman et al., 2018) for C16orf71. Digested peptides were desalted with Hypersep Spin Tip C-18 columns (Thermo Scientific), dried, and resuspended in 30-60 µl of 5% acetonitrile, 0.1% acetic acid for mass spectrometry.

Samples from experiments with baits Dnai2 and Wdr78 were analyzed on a Thermo Orbitrap Fusion mass spectrometer and those with bait C16orf71 were analyzed using a Thermo Orbitrap Fusion Lumos Tribrid mass spectrometer. In all cases peptides were separated using reverse phase chromatography on a Dionex Ultimate 3000 RSLCnano UHPLC system (Thermo Scientific) with a C18 trap to Acclaim C18 PepMap RSLC column (Dionex; Thermo Scientific)

configuration and eluted using a 3 to 45% gradient over 60 min. with direct injection into the mass spectrometer using nano-electrospray. Data were collected using a data-dependent top speed HCD acquisition method with full precursor ion scans (MS1) collected at 120,000 m/z resolution. Monoisotopic precursor selection and charge-state screening were enabled using Advanced Peak Determination (APD), with ions of charge ≥ + 2 selected for high energy-induced dissociation (HCD) with stepped collision energy of 30% +/- 3% (Lumos) or 31% +/- 4% (Orbitrap Fusion). Dynamic exclusion was active for ions selected once with an exclusion period of 20 sec (Lumos) or 30 sec (Orbitrap Fusion). All MS2 scans were centroid and collected in rapid mode.

Raw MS/MS spectra were processed using Proteome Discoverer (v2.3). We used the Percolator node in Proteome Discoverer to assign unique peptide spectral matches (PSMs) at FDR < 5% to the composite form of the *X. laevis* reference proteome described in (Drew et al., 2020), which comprises both genome-derived Xenbase JGI v9.1 + GenBank *X. laevis* protein sets, but with homeologs and highly related entries combined into EggNOG vertebrate-level orthology groups (Huerta-Cepas et al., 2016), based on the method developed in (McWhite et al., 2020). In order to identify proteins statistically significantly associated with each bait, we calculated both a $\log_2$ fold-change and a Z-score for each protein based on the observed PSMs in the bait ('expt') versus control ('ctrl') pulldown. The fold-change was computed for each protein as:

$$FC_{protein\ i} = \log_2\left(\frac{(PSM_{i,expt}+1)/\sum_{j=1}^{n}(PSM_{j,expt}+1)}{(PSM_{i,ctrl}+1)/\sum_{k=1}^{n}(PSM_{k,ctrl}+1)}\right),$$

where *n* is the total number of proteins considered in the experiment.

We calculated significance for protein enrichment in the experiment relative to control using a one-sided Z-test as in (Lu et al., 2007) with a 90% confidence threshold (z ≥ 1.282), as:

$$Z_{protein\ i} = \frac{f_{i,expt} - f_{i,ctrl}}{\sqrt{\frac{f_{i,comb}(1-f_{i,comb})}{\sum_{j=1}^{n} PSM_{j,expt}} + \frac{f_{i,comb}(1-f_{i,comb})}{\sum_{j=1}^{n} PSM_{j,ctrl}}}},$$

where fi=PSMi/j=1nPSMj and fi,comb=(PSMi,expt+PSMi,ctrl)/j=1n(PSMj,expt+PSMj,ctrl).

Imaging, FRAP and image analysis: Embryos injected with mRNA encoding Halo-tagged proteins were labeled with Halo ligand conjugated Janelia Fluor 646 (Promega, cat# GA1121) at room temperature for 30 min and then were imaged after washing. For live imaging, *Xenopus* embryos were mounted between cover glass and submerged in 1/3x MMR at stage 23. Images were captured with a Zeiss LSM700 laser scanning confocal microscope using a plan-apochromat 63X 1.4 NA oil objective lens (Zeiss). For FRAP experiments, a region of interest (ROI) was defined as a 1.75 µm X 1.75 µm box. ROIs were bleached using 50% laser power of a 488-nm laser and a 0.64 µsec pixel dwell time. Fluorescence recovery was recorded at ~0.20 second intervals for up to 300 frames. Bleach correction and FRAP curve-fitting was carried out using a custom python script (modified from http://imagej.net/Analyze_FRAP_movies_with_a_Jython_script). Plots were generated using PRISM 8.

Protein domain prediction: The human C16orf71 sequence was analyzed using the PSIPRED Protein Analysis Workbench for disorder and secondary structure prediction (Buchan and Jones, 2019).

Airway epithelial cell culture and Immunostaining**:** Human trachea were isolated from surgical excess of tracheobronchial segments of lungs donated for transplantation. These unidentified tissues are exempt from regulation by HHS regulation 45 CFR Part 46. Paraffin embedded tracheal sections were fixed and immunostained as previously described (Pan et al., 2007; You et al., 2002). Nuclei were stained using 4', 6-diamidino-2-phenylindole (DAPI, Vector Laboratories, Burlingame, CA, USA). The ODA protein, DNAI1, was detected using primary antibodies obtained from NeuroMab (UC Davis, Ca, clone UNC 65.56.18.11). Antibodies to Daap1 (C16orf71) were obtained from Sigma-Millipore (St. Louis, MO, HPA049468). Images were acquired using a Zeiss LSM700 laser scanning confocal microscope.

In situ hybridization: *In situ* hybridization was performed as described previously (Sive et al., 2000). Bright field images were captured with a Zeiss Axio Zoom. V16 stereo microscope with Carl Zeiss Axiocam HRc color microscope camera.

RT-PCR**:** To verify the efficiency of *C16orf71* MOs, MOs were injected into all cells at the 4-cell stage and total RNA was isolated using the TRIZOL reagent (Invitrogen) at stage 23. cDNA was synthesized using M-MLV Reverse Transcriptase (Invitrogen) and random hexamers. C16orf71 cDNAs were amplified by Taq polymerase (NEB) with these primers: c16orf71 5F 5'-cttcagagcaggacggattt-3', c16orf71 582R 5'-ggcagaggtgcttagatgtt-3', c16orf71 600F 5'- gggcttgtcattgcagtttc-3', c16orf71 1254R 5'-tctctaccgtccttctcttctc-3'. ODC primers were ODC 426F 5'-ggcaaggaatcacccgaatg-3' and ODC 843R 5'-ggcaacatagtatctcccaggctc-3'.

Data Deposition: Proteomics data has been deposited in the PRIDE repository with accession PXD017980.

References

Anderegg, L., M. Im Hof Gut, U. Hetzel, E.W. Howerth, F. Leuthard, K. Kyostila, H. Lohi, L. Pettitt, C. Mellersh, K.M. Minor, J.R. Mickelson, K. Batcher, D. Bannasch, V. Jagannathan, and T. Leeb. 2019. NME5 frameshift variant in Alaskan Malamutes with primary ciliary dyskinesia. *PLoS Genet*. 15:e1008378.

Ariizumi, T., S. Takahashi, T.c. Chan, Y. Ito, T. Michiue, and M. Asashima. 2009. Isolation and differentiation of Xenopus animal cap cells. *Current protocols in stem cell biology*. 9:1D. 5.1-1D. 5.31.

Banani, S.F., H.O. Lee, A.A. Hyman, and M.K. Rosen. 2017. Biomolecular condensates: organizers of cellular biochemistry. *Nat Rev Mol Cell Biol*. 18:285-298.

Buchan, D.W.A., and D.T. Jones. 2019. The PSIPRED Protein Analysis Workbench: 20 years on. *Nucleic Acids Res*. 47:W402-w407.

Cho, K.J., S.H. Noh, S.M. Han, W.I. Choi, H.Y. Kim, S. Yu, J.S. Lee, J.H. Rim, M.G. Lee, F. Hildebrandt, and H.Y. Gee. 2018. ZMYND10 stabilizes intermediate chain proteins in the cytoplasmic pre-assembly of dynein arms. *PLoS Genet*. 14:e1007316.

Chung, M.I., T. Kwon, F. Tu, E.R. Brooks, R. Gupta, M. Meyer, J.C. Baker, E.M. Marcotte, and J.B. Wallingford. 2014. Coordinated genomic control of ciliogenesis and cell movement by RFX2. *Elife*. 3:e01439.

Deblandre, G.A., D.A. Wettstein, N. Koyano-Nakagawa, and C. Kintner. 1999. A two-step mechanism generates the spacing pattern of the ciliated cells in the skin of Xenopus embryos. *Development*. 126:4715-4728.

Desai, P.B., A.B. Dean, and D.R. Mitchell. 2018. Cytoplasmic preassembly and trafficking of axonemal dyneins. *In* Dyneins: Structure, Biology, and Disease. Vol. 1. S.M. King, editor. Academic Press/Elsevier, London.

Desvignes, T., P. Pontarotti, C. Fauvel, and J. Bobe. 2009. Nme protein family evolutionary history, a vertebrate perspective. *BMC evolutionary biology*. 9:256.

Diggle, C.P., D.J. Moore, G. Mali, P. zur Lage, A. Ait-Lounis, M. Schmidts, A. Shoemark, A. Garcia Munoz, M.R. Halachev, P. Gautier, P.L. Yeyati, D.T. Bonthron, I.M. Carr, B. Hayward, A.F. Markham, J.E. Hope, A. von Kriegsheim, H.M. Mitchison, I.J. Jackson, B. Durand, W. Reith, E. Sheridan, A.P. Jarman, and P. Mill. 2014. HEATR2 plays a conserved role in assembly of the ciliary motile apparatus. *PLoS Genet*. 10:e1004577.

Dougherty, G.W., N.T. Loges, J.A. Klinkenbusch, H. Olbrich, P. Pennekamp, T. Menchen, J. Raidt, J. Wallmeier, C. Werner, C. Westermann, C. Ruckert, V. Mirra, R. Hjeij, Y. Memari, R. Durbin, A. Kolb-Kokocinski, K. Praveen, M.A. Kashef, S. Kashef, F. Eghtedari, K. Haffner, P. Valmari, G. Baktai, M. Aviram, L. Bentur, I. Amirav, E.E. Davis, N. Katsanis, M. Brueckner, A. Shaposhnykov, G. Pigino, B. Dworniczak, and H. Omran. 2016. DNAH11 Localization in the Proximal Region of Respiratory Cilia Defines Distinct Outer Dynein Arm Complexes. *Am. J. Respir. Cell Mol. Biol.* 55:213-224.

Drew, K., C. Lee, V. Dang, O. Papoulas, R.M. Cox, R.L. Huizar, E.M. Marcotte, and J.B. Wallingford. 2020. A systematic, label-free method for identifying RNA-associated proteins in vivo provides insights into ciliary beating. *BioRxiv*.

Duriez, B., P. Duquesnoy, E. Escudier, A.-M. Bridoux, D. Escalier, I. Rayet, E. Marcos, A.-M. Vojtek, J.-F. Bercher, and S. Amselem. 2007. A common variant in combination with a

nonsense mutation in a member of the thioredoxin family causes primary ciliary dyskinesia. *Proceedings of the National Academy of Sciences*. 104:3336-3341.

Fabczak, H., and A. Osinka. 2019. Role of the Novel Hsp90 Co-Chaperones in Dynein Arms' Preassembly. *International journal of molecular sciences*. 20:6174.

Feric, M., N. Vaidya, T.S. Harmon, D.M. Mitrea, L. Zhu, T.M. Richardson, R.W. Kriwacki, R.V. Pappu, and C.P. Brangwynne. 2016. Coexisting Liquid Phases Underlie Nucleolar Subcompartments. *Cell*. 165:1686-1697.

Fliegauf, M., H. Olbrich, J. Horvath, J.H. Wildhaber, M.A. Zariwala, M. Kennedy, M.R. Knowles, and H. Omran. 2005. Mislocalization of DNAH5 and DNAH9 in respiratory cells from patients with primary ciliary dyskinesia. *Am. J. Respir. Crit. Care Med.* 171:1343-1349.

Fowkes, M.E., and D.R. Mitchell. 1998. The role of preassembled cytoplasmic complexes in assembly of flagellar dynein subunits. *Mol. Biol. Cell*. 9:2337-2347.

Fu, G., Q. Wang, N. Phan, P. Urbanska, E. Joachimiak, J. Lin, D. Wloga, and D. Nicastro. 2018. The I1 dynein-associated tether and tether head complex is a conserved regulator of ciliary motility. *Mol. Biol. Cell*. 29:1048-1059.

Gao, W., L. Xu, R. Guan, X. Liu, Y. Han, Q. Wu, Y. Xiao, F. Qi, Z. Zhu, and S. Lin. 2011. Wdr18 is required for Kupffer's vesicle formation and regulation of body asymmetry in zebrafish. *PLoS ONE*. 6:e23386.

Goodman, J.K., C.G. Zampronio, A.M.E. Jones, and J.R. Hernandez-Fernaud. 2018. Updates of the In-Gel Digestion Method for Protein Analysis by Mass Spectrometry. *Proteomics*. 18:e1800236.

Hayes, J.M., S.K. Kim, P.B. Abitua, T.J. Park, E.R. Herrington, A. Kitayama, M.W. Grow, N. Ueno, and J.B. Wallingford. 2007. Identification of novel ciliogenesis factors using a new in vivo model for mucociliary epithelial development. *Dev. Biol.* 312:115-130.

Horani, A., T.E. Druley, M.A. Zariwala, A.C. Patel, B.T. Levinson, L.G. Van Arendonk, K.C. Thornton, J.C. Giacalone, A.J. Albee, K.S. Wilson, E.H. Turner, D.A. Nickerson, J. Shendure, P.V. Bayly, M.W. Leigh, M.R. Knowles, S.L. Brody, S.K. Dutcher, and T.W. Ferkol. 2012. Whole-exome capture and sequencing identifies HEATR2 mutation as a cause of primary ciliary dyskinesia. *Am. J. Hum. Genet.* 91:685-693.

Horani, A., T.W. Ferkol, S.K. Dutcher, and S.L. Brody. 2016. Genetics and biology of primary ciliary dyskinesia. *Paediatr Respir Rev*. 18:18-24.

Horani, A., T.W. Ferkol, D. Shoseyov, M.G. Wasserman, Y.S. Oren, B. Kerem, I. Amirav, M. Cohen-Cymberknoh, S.K. Dutcher, S.L. Brody, O. Elpeleg, and E. Kerem. 2013. LRRC6 mutation causes primary ciliary dyskinesia with dynein arm defects. *PLoS ONE*. 8:e59436.

Horani, A., A. Ustione, T. Huang, A.L. Firth, J. Pan, S.P. Gunsten, J.A. Haspel, D.W. Piston, and S.L. Brody. 2018. Establishment of the early cilia preassembly protein complex during motile ciliogenesis. *Proc. Natl. Acad. Sci. U. S. A.* 115:E1221-E1228.

Huerta-Cepas, J., D. Szklarczyk, K. Forslund, H. Cook, D. Heller, M.C. Walter, T. Rattei, D.R. Mende, S. Sunagawa, M. Kuhn, L.J. Jensen, C. von Mering, and P. Bork. 2016. eggNOG 4.5: a hierarchical orthology framework with improved functional annotations for eukaryotic, prokaryotic and viral sequences. *Nucleic Acids Res*. 44:D286-293.

Huizar, R.L., C. Lee, A.A. Boulgakov, A. Horani, F. Tu, E.M. Marcotte, S.L. Brody, and J.B. Wallingford. 2018. A liquid-like organelle at the root of motile ciliopathy. *Elife*. 7.

Jain, S., J.R. Wheeler, R.W. Walters, A. Agrawal, A. Barsic, and R. Parker. 2016. ATPase-Modulated Stress Granules Contain a Diverse Proteome and Substructure. *Cell*. 164:487-498.

Kamiya, R., and T. Yagi. 2014. Functional diversity of axonemal dyneins as assessed by in vitro and in vivo motility assays of Chlamydomonas mutants. *Zoolog. Sci.* 31:633-645.

Karimi, K., J.D. Fortriede, V.S. Lotay, K.A. Burns, D.Z. Wang, M.E. Fisher, T.J. Pells, C. James-Zorn, Y. Wang, V.G. Ponferrada, S. Chu, P. Chaturvedi, A.M. Zorn, and P.D. Vize. 2018. Xenbase: a genomic, epigenomic and transcriptomic model organism database. *Nucleic Acids Res*. 46:D861-D868.

Kim, S., L. Ma, M.N. Shokhirev, I. Quigley, and C. Kintner. 2018. Multicilin and activated E2f4 induce multiciliated cell differentiation in primary fibroblasts. *Sci Rep*. 8:12369.

King, S.M. 2018a. Composition and assembly of axonemal dyneins. *In* Dyneins: Structure, Biology, and Disease. S.M. King, editor. Academic Press/Elsevier, London. 162-201.

King, S.M. 2018b. Composition and assembly of axonemal dyneins. *In* Dyneins. Elsevier. 162-201.

Kott, E., P. Duquesnoy, B. Copin, M. Legendre, F. Dastot-Le Moal, G. Montantin, L. Jeanson, A. Tamalet, J.F. Papon, J.P. Siffroi, N. Rives, V. Mitchell, J. de Blic, A. Coste, A. Clement, D. Escalier, A. Toure, E. Escudier, and S. Amselem. 2012. Loss-of-function mutations in LRRC6, a gene essential for proper axonemal assembly of inner and outer dynein arms, cause primary ciliary dyskinesia. *Am. J. Hum. Genet.* 91:958-964.

Kramer, A., F. Ferfoglia, C.J. Huang, F. Mulhaupt, D. Nesic, and G. Tanackovic. 2005. Structure-function analysis of the U2 snRNP-associated splicing factor SF3a. *Biochem. Soc. Trans.* 33:439-442.

Kubo, T., Y. Hou, D.A. Cochran, G.B. Witman, and T. Oda. 2018. A microtubule-dynein tethering complex regulates the axonemal inner dynein f (I1). *Mol. Biol. Cell*. 29:1060-1074.

Li, Y., L. Zhao, S. Yuan, J. Zhang, and Z. Sun. 2017. Axonemal dynein assembly requires the R2TP complex component Pontin. *Development*. 144:4684-4693.

Lin, Y., D.S. Protter, M.K. Rosen, and R. Parker. 2015. Formation and Maturation of Phase-Separated Liquid Droplets by RNA-Binding Proteins. *Mol. Cell*. 60:208-219.

Lu, P., C. Vogel, R. Wang, X. Yao, and E.M. Marcotte. 2007. Absolute protein expression profiling estimates the relative contributions of transcriptional and translational regulation. *Nat. Biotechnol.* 25:117-124.

Ma, L., I. Quigley, H. Omran, and C. Kintner. 2014. Multicilin drives centriole biogenesis via E2f proteins. *Genes Dev.* 28:1461-1471.

Mali, G.R., P.L. Yeyati, S. Mizuno, D.O. Dodd, P.A. Tennant, M.A. Keighren, P. Zur Lage, A. Shoemark, A. Garcia-Munoz, A. Shimada, H. Takeda, F. Edlich, S. Takahashi, A. von Kreigsheim, A.P. Jarman, and P. Mill. 2018. ZMYND10 functions in a chaperone relay during axonemal dynein assembly. *Elife*. 7.

McWhite, C.D., O. Papoulas, K. Drew, R.M. Cox, V. June, O.X. Dong, T. Kwon, C. Wan, M.L. Salmi, S.J. Roux, K.S. Browning, Z.J. Chen, P.C. Ronald, and E.M. Marcotte. 2020. A Pan-plant Protein Complex Map Reveals Deep Conservation and Novel Assemblies. *Cell*. 181:460-474.e414.

Mitchison, H.M., M. Schmidts, N.T. Loges, J. Freshour, A. Dritsoula, R.A. Hirst, C. O'Callaghan, H. Blau, M. Al Dabbagh, H. Olbrich, P.L. Beales, T. Yagi, H. Mussaffi, E.M. Chung, H. Omran,

and D.R. Mitchell. 2012. Mutations in axonemal dynein assembly factor DNAAF3 cause primary ciliary dyskinesia. *Nat. Genet.* 44:381-389, S381-382.

Mitchison, H.M., and E.M. Valente. 2017. Motile and non-motile cilia in human pathology: from function to phenotypes. *J. Pathol.* 241:294-309.

Mittag, T., and R. Parker. 2018. Multiple Modes of Protein-Protein Interactions Promote RNP Granule Assembly. *J. Mol. Biol.* 430:4636-4649.

Moore, D.J., A. Onoufriadis, A. Shoemark, M.A. Simpson, P.I. zur Lage, S.C. de Castro, L. Bartoloni, G. Gallone, S. Petridi, W.J. Woollard, D. Antony, M. Schmidts, T. Didonna, P. Makrythanasis, J. Bevillard, N.P. Mongan, J. Djakow, G. Pals, J.S. Lucas, J.K. Marthin, K.G. Nielsen, F. Santoni, M. Guipponi, C. Hogg, S.E. Antonarakis, R.D. Emes, E.M. Chung, N.D. Greene, J.L. Blouin, A.P. Jarman, and H.M. Mitchison. 2013. Mutations in ZMYND10, a gene essential for proper axonemal assembly of inner and outer dynein arms in humans and flies, cause primary ciliary dyskinesia. *Am. J. Hum. Genet.* 93:346-356.

Olcese, C., M.P. Patel, A. Shoemark, S. Kiviluoto, M. Legendre, H.J. Williams, C.K. Vaughan, J. Hayward, A. Goldenberg, R.D. Emes, M.M. Munye, L. Dyer, T. Cahill, J. Bevillard, C. Gehrig, M. Guipponi, S. Chantot, P. Duquesnoy, L. Thomas, L. Jeanson, B. Copin, A. Tamalet, C. Thauvin-Robinet, J.F. Papon, A. Garin, I. Pin, G. Vera, P. Aurora, M.R. Fassad, L. Jenkins, C. Boustred, T. Cullup, M. Dixon, A. Onoufriadis, A. Bush, E.M. Chung, S.E. Antonarakis, M.R. Loebinger, R. Wilson, M. Armengot, E. Escudier, C. Hogg, U.K.R. Group, S. Amselem, Z. Sun, L. Bartoloni, J.L. Blouin, and H.M. Mitchison. 2017. X-linked primary ciliary dyskinesia due to mutations in the cytoplasmic axonemal dynein assembly factor PIH1D3. *Nat Commun*. 8:14279.

Omran, H., D. Kobayashi, H. Olbrich, T. Tsukahara, N.T. Loges, H. Hagiwara, Q. Zhang, G. Leblond, E. O'Toole, C. Hara, H. Mizuno, H. Kawano, M. Fliegauf, T. Yagi, S. Koshida, A. Miyawaki, H. Zentgraf, H. Seithe, R. Reinhardt, Y. Watanabe, R. Kamiya, D.R. Mitchell, and H. Takeda. 2008. Ktu/PF13 is required for cytoplasmic pre-assembly of axonemal dyneins. *Nature*. 456:611-616.

Paff, T., N.T. Loges, I. Aprea, K. Wu, Z. Bakey, E.G. Haarman, J.M. Daniels, E.A. Sistermans, N. Bogunovic, G.W. Dougherty, I.M. Hoben, J. Grosse-Onnebrink, A. Matter, H. Olbrich, C. Werner, G. Pals, M. Schmidts, H. Omran, and D. Micha. 2017. Mutations in PIH1D3 Cause X-Linked Primary Ciliary Dyskinesia with Outer and Inner Dynein Arm Defects. *Am. J. Hum. Genet.* 100:160-168.

Pan, J., Y. You, T. Huang, and S.L. Brody. 2007. RhoA-mediated apical actin enrichment is required for ciliogenesis and promoted by Foxj1. *J. Cell Sci.* 120:1868-1876.

Pazour, G.J., N. Agrin, B.L. Walker, and G.B. Witman. 2006. Identification of predicted human outer dynein arm genes: candidates for primary ciliary dyskinesia genes. *J. Med. Genet.* 43:62-73.

Quigley, I.K., and C. Kintner. 2017. Rfx2 Stabilizes Foxj1 Binding at Chromatin Loops to Enable Multiciliated Cell Gene Expression. *PLoS Genet*. 13:e1006538.

Sadek, C.M., A. Jiménez, A.E. Damdimopoulos, T. Kieselbach, M. Nord, J.-Å. Gustafsson, G. Spyrou, E.C. Davis, R. Oko, and F.A. Van der Hoorn. 2003. Characterization of human thioredoxin-like 2 A novel microtubule-binding thioredoxin expressed predominantly in the cilia of lung airway epithelium and spermatid manchette and axoneme. *J. Biol. Chem.* 278:13133-13142.

Schmidt, H.B., and R. Rohatgi. 2016. In Vivo Formation of Vacuolated Multi-phase Compartments Lacking Membranes. *Cell Rep*. 16:1228-1236.

Session, A.M., Y. Uno, T. Kwon, J.A. Chapman, A. Toyoda, S. Takahashi, A. Fukui, A. Hikosaka, A. Suzuki, M. Kondo, S.J. van Heeringen, I. Quigley, S. Heinz, H. Ogino, H. Ochi, U. Hellsten, J.B. Lyons, O. Simakov, N. Putnam, J. Stites, Y. Kuroki, T. Tanaka, T. Michiue, M. Watanabe, O. Bogdanovic, R. Lister, G. Georgiou, S.S. Paranjpe, I. van Kruijsbergen, S. Shu, J. Carlson, T. Kinoshita, Y. Ohta, S. Mawaribuchi, J. Jenkins, J. Grimwood, J. Schmutz, T. Mitros, S.V. Mozaffari, Y. Suzuki, Y. Haramoto, T.S. Yamamoto, C. Takagi, R. Heald, K. Miller, C. Haudenschild, J. Kitzman, T. Nakayama, Y. Izutsu, J. Robert, J. Fortriede, K. Burns, V. Lotay, K. Karimi, Y. Yasuoka, D.S. Dichmann, M.F. Flajnik, D.W. Houston, J. Shendure, L. DuPasquier, P.D. Vize, A.M. Zorn, M. Ito, E.M. Marcotte, J.B. Wallingford, Y. Ito, M. Asashima, N. Ueno, Y. Matsuda, G.J. Veenstra, A. Fujiyama, R.M. Harland, M. Taira, and D.S. Rokhsar. 2016. Genome evolution in the allotetraploid frog Xenopus laevis. *Nature*. 538:336-343.

Shin, Y., and C.P. Brangwynne. 2017. Liquid phase condensation in cell physiology and disease. *Science*. 357.

Silversides, C.K., A.C. Lionel, G. Costain, D. Merico, O. Migita, B. Liu, T. Yuen, J. Rickaby, B. Thiruvahindrapuram, and C.R. Marshall. 2012. Rare copy number variations in adults with tetralogy of Fallot implicate novel risk gene pathways. *PLoS genetics*. 8:e1002843.

Sive, H.L., R.M. Grainger, and R.M. Harland. 2000. Early Development of Xenopus laevis: A Laboratory Manual. Cold Spring Harbor Press, Cold Spring Harbor, N.Y.

Soares, H., B. Carmona, S. Nolasco, L. Viseu Melo, and J. Goncalves. 2019. Cilia Distal Domain: Diversity in Evolutionarily Conserved Structures. *Cells*. 8.

Tarkar, A., N.T. Loges, C.E. Slagle, R. Francis, G.W. Dougherty, J.V. Tamayo, B. Shook, M. Cantino, D. Schwartz, C. Jahnke, H. Olbrich, C. Werner, J. Raidt, P. Pennekamp, M. Abouhamed, R. Hjeij, G. Kohler, M. Griese, Y. Li, K. Lemke, N. Klena, X. Liu, G. Gabriel, K. Tobita, M. Jaspers, L.C. Morgan, A.J. Shapiro, S.J. Letteboer, D.A. Mans, J.L. Carson, M.W. Leigh, W.E. Wolf, S. Chen, J.S. Lucas, A. Onoufriadis, V. Plagnol, M. Schmidts, K. Boldt, R. Roepman, M.A. Zariwala, C.W. Lo, H.M. Mitchison, M.R. Knowles, R.D. Burdine, J.J. Loturco, and H. Omran. 2013. DYX1C1 is required for axonemal dynein assembly and ciliary motility. *Nat. Genet.* 45:995-1003.

Tu, F., J. Sedzinski, Y. Ma, E.M. Marcotte, and J.B. Wallingford. 2018. Protein localization screening in vivo reveals novel regulators of multiciliated cell development and function. *J. Cell Sci.* 131.

Uhlén, M., L. Fagerberg, B.M. Hallström, C. Lindskog, P. Oksvold, A. Mardinoglu, Å. Sivertsson, C. Kampf, E. Sjöstedt, and A. Asplund. 2015. Tissue-based map of the human proteome. *Science*. 347:1260419.

Vogel, P., R.W. Read, G.M. Hansen, B.J. Payne, D. Small, A.T. Sands, and B.P. Zambrowicz. 2012. Congenital hydrocephalus in genetically engineered mice. *Vet. Pathol.* 49:166-181.

Walentek, P., and I.K. Quigley. 2017. What we can learn from a tadpole about ciliopathies and airway diseases: Using systems biology in Xenopus to study cilia and mucociliary epithelia. *Genesis*. 55.

Walentek, P., I.K. Quigley, D.I. Sun, U.K. Sajjan, C. Kintner, and R.M. Harland. 2016. Ciliary transcription factors and miRNAs precisely regulate Cp110 levels required for ciliary adhesions and ciliogenesis. *Elife*. 5.

Werner, M.E., and B.J. Mitchell. 2011. Understanding ciliated epithelia: The power of Xenopus. *Genesis*.

Werner, M.E., and B.J. Mitchell. 2012. Understanding ciliated epithelia: the power of Xenopus. *Genesis*. 50:176-185.

Yamaguchi, H., T. Oda, M. Kikkawa, and H. Takeda. 2018. Systematic studies of all PIH proteins in zebrafish reveal their distinct roles in axonemal dynein assembly. *eLife*. 7:e36979.

Yamamoto, R., M. Hirono, and R. Kamiya. 2010. Discrete PIH proteins function in the cytoplasmic preassembly of different subsets of axonemal dyneins. *J. Cell Biol.* 190:65-71.

You, Y., E.J. Richer, T. Huang, and S.L. Brody. 2002. Growth and differentiation of mouse tracheal epithelial cells: selection of a proliferative population. *Am J Physiol Lung Cell Mol Physiol*. 283:L1315-1321.

Zariwala, M.A., H.Y. Gee, M. Kurkowiak, D.A. Al-Mutairi, M.W. Leigh, T.W. Hurd, R. Hjeij, S.D. Dell, M. Chaki, G.W. Dougherty, M. Adan, P.C. Spear, J. Esteve-Rudd, N.T. Loges, M. Rosenfeld, K.A. Diaz, H. Olbrich, W.E. Wolf, E. Sheridan, T.F. Batten, J. Halbritter, J.D. Porath, S. Kohl, S. Lovric, D.Y. Hwang, J.E. Pittman, K.A. Burns, T.W. Ferkol, S.D. Sagel, K.N. Olivier, L.C. Morgan, C. Werner, J. Raidt, P. Pennekamp, Z. Sun, W. Zhou, R. Airik, S. Natarajan, S.J. Allen, I. Amirav, D. Wieczorek, K. Landwehr, K. Nielsen, N. Schwerk, J. Sertic, G. Kohler, J. Washburn, S. Levy, S. Fan, C. Koerner-Rettberg, S. Amselem, D.S. Williams, B.J. Mitchell, I.A. Drummond, E.A. Otto, H. Omran, M.R. Knowles, and F. Hildebrandt. 2013. ZMYND10 is mutated in primary ciliary dyskinesia and interacts with LRRC6. *Am. J. Hum. Genet.* 93:336-345.

Zhang, Y., Y. Chen, J. Zheng, J. Wang, S. Duan, W. Zhang, X. Yan, and X. Zhu. 2019. Vertebrate Dynein-f depends on Wdr78 for axonemal localization and is essential for ciliary beat. *J Mol Cell Biol*. 11:383-394.

Zhao, L., S. Yuan, Y. Cao, S. Kallakuri, Y. Li, N. Kishimoto, L. DiBella, and Z. Sun. 2013. Reptin/Ruvbl2 is a Lrrc6/Seahorse interactor essential for cilia motility. *Proc. Natl. Acad. Sci. U. S. A.* 110:12697-12702.

Zur Lage, P., P. Stefanopoulou, K. Styczynska-Soczka, N. Quinn, G. Mali, A. von Kriegsheim, P. Mill, and A.P. Jarman. 2018. Ciliary dynein motor preassembly is regulated by Wdr92 in association with HSP90 co-chaperone, R2TP. *J. Cell Biol.* 217:2583-2598.

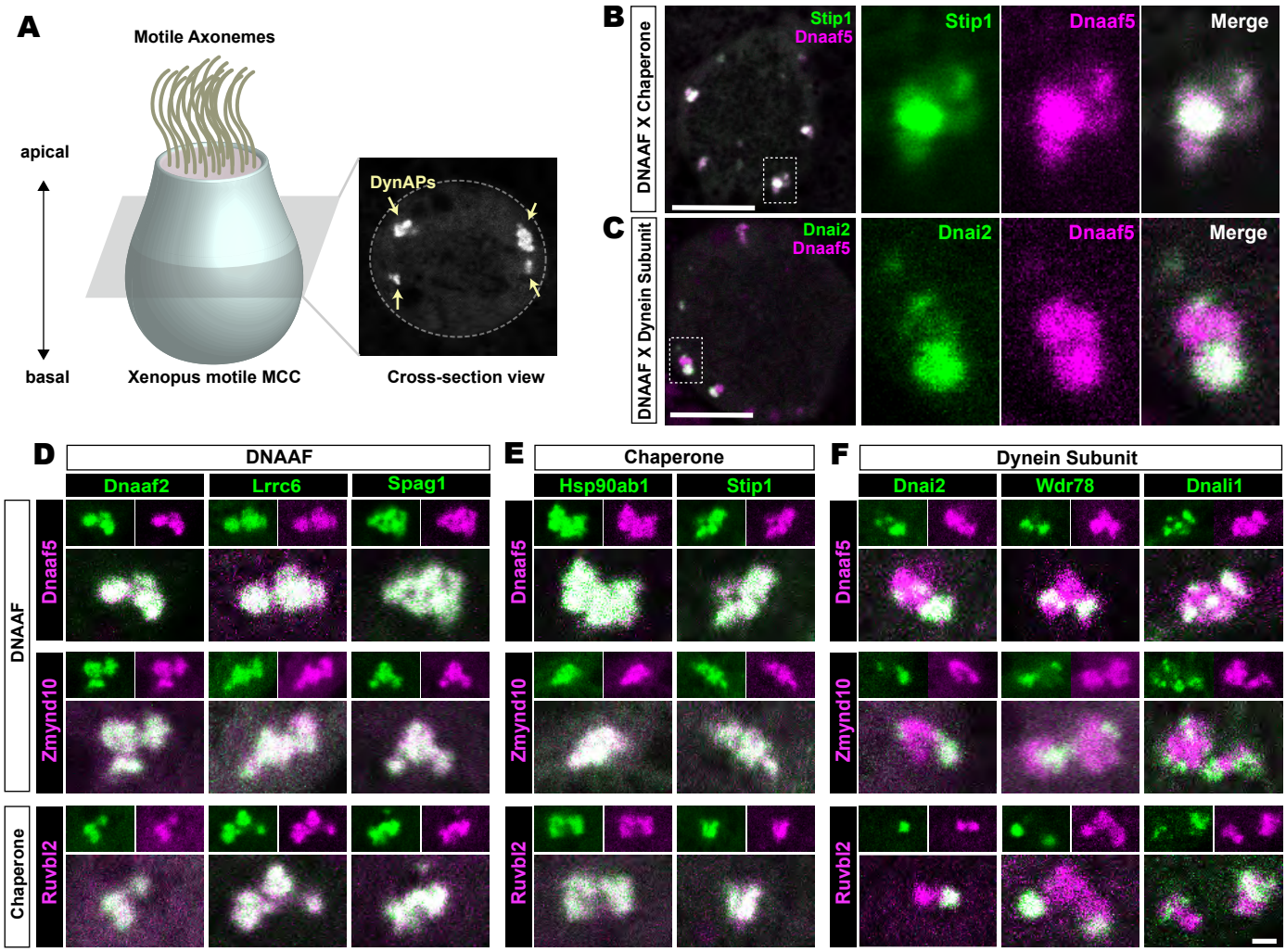

Lee et al., Figure 1

Figure 1. Dynein subunits occupy sub-regions within DynAPs.
A. Schematic showing an MCC and a representative *en face* optical section through the cytoplasm showing DynAPs. **B.** *En face optical* section through the cytoplasm of a *Xenopus* MCC expressing GFP-Stip1 (a chaperone, green) and mCherry-Dnaaf5 (a DNAAF, magenta). Note near-perfect co-localization. Dashed box indicates region shown in high magnification, split-channel views at right. Scale bar=10 μm. **C.** GFP-Dnai2 (a dynein subunit, green) co-localizes only partially with mCherry-Dnaaf5. **D, E.** Images of pairwise labeling of individual DynAPs with the indicated tagged DNAAFs or chaperones. Smaller panels show split channels, larger images show the merged channels. Note high degree of co-localization. **F.** Similar pair-wise labelling with dynein subunits reveals only partial co-localization. Scale bar=1 μm.

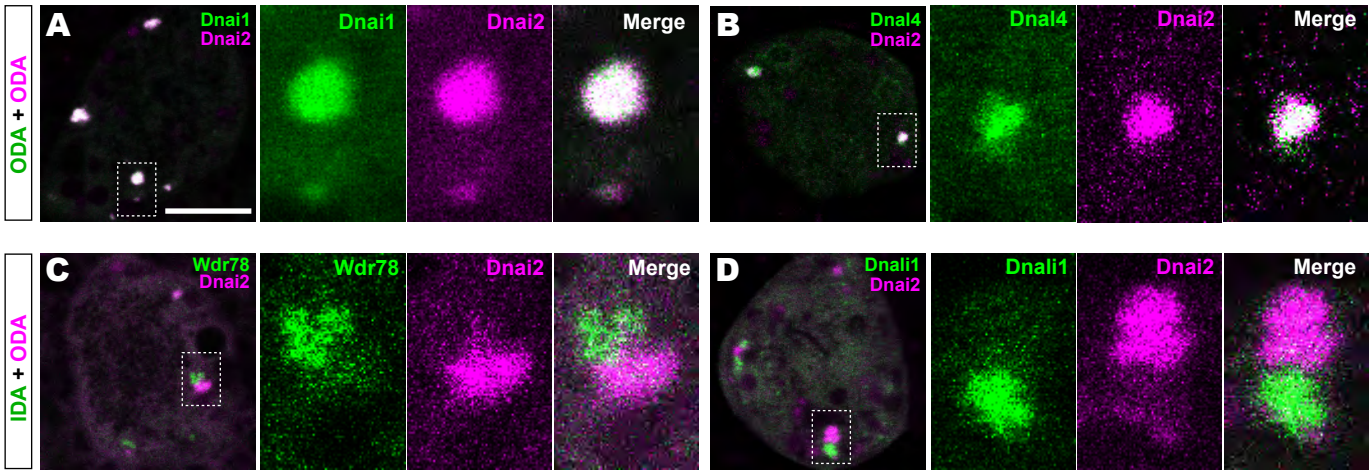

Lee et al., Figure 2

Figure 2. Outer and inner dynein arms localize to distinct sub-regions in DynAPs.
A. *En face* optical section of a *Xenopus* MCC expressing ODA subunits GFP-Dnai1 and RFP-Dnai2, note near complete co-localization. Higher magnification view of area in dashed box is shown at right. **B.** Dnai2-RFP also displays near-total co-localization with another ODA subunit, Dnal4. **C, D.** Dnai2-GFP shows very little co-localization with the IDA subunit GFP-Wdr78 or GFP-Dnali1. Scale bar = 10 μm.

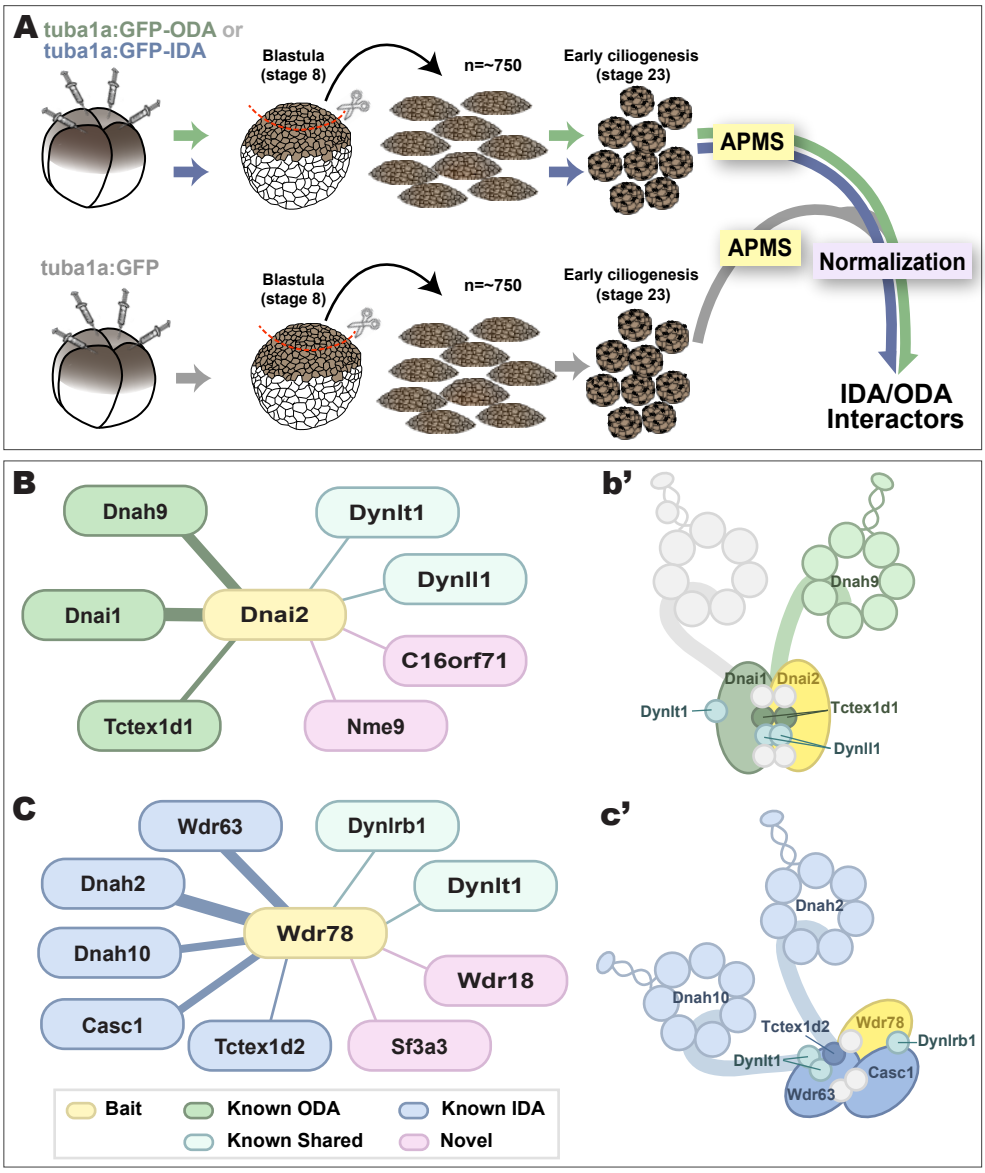

Lee et al., Figure 3

Figure 3. Specific identification of outer and inner arm dynein interactors.
A. Schematic of APMS workflow for identifying *in vivo* ODA and IDA interactors. GFP tagged ODA or IDA driven by MCC-specific a-tubulin promoter by plasmid injection into *Xenopus* embryos and animal caps were isolated at stage 8. The cultured explants were collected at early ciliogenesis stage (stage 23) and subjected to APMS. Unfused GFP was assessed simultaneously and the data subtracted to control for non-specific interactions. **B.** Spoke diagram displaying Dnai2 (ODA) interactors, line weight of spokes indicates Log2 fold-change of PSMs. **C.** Schematic of outer dynein arm indicating identified Dnai2 preys. **B.** Spoke diagram displaying Wdr78 (IDA) interactors. **C.** Schematic of inner dynein arm (f type) indicating identified Wdr78 preys.

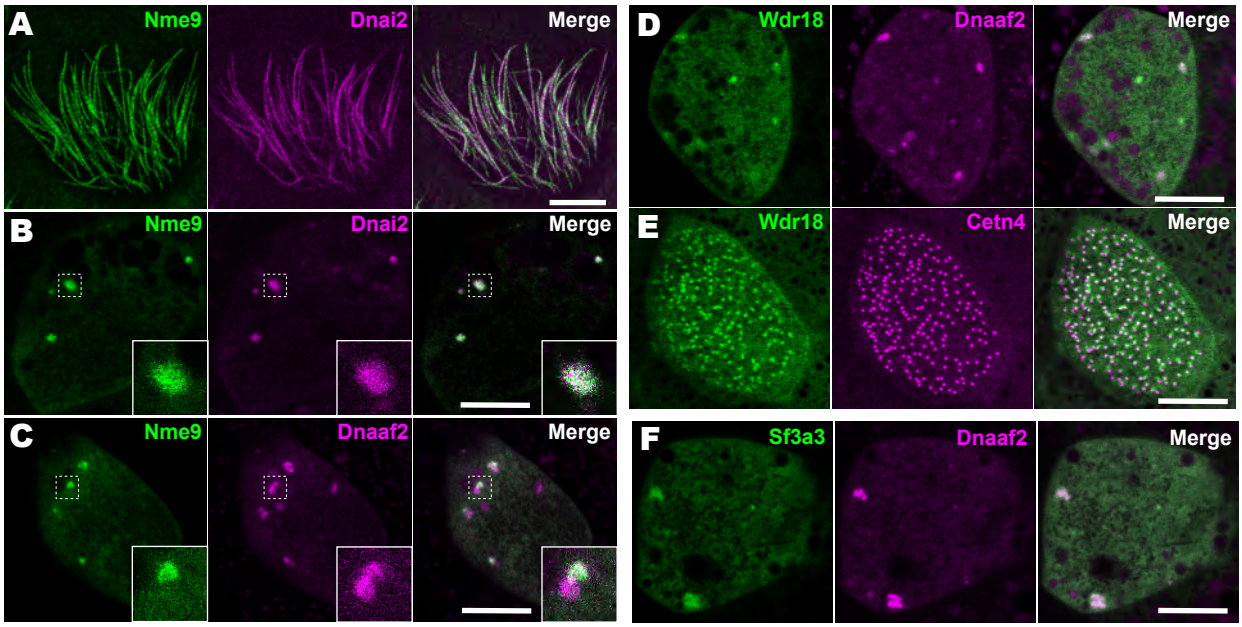

Lee et al., Figure 4

Figure 4. Localization of novel IDA and ODA interactors.
A. *En face* optical section just above the apical surface of a *Xenopus* MCC showing axonemal localization of GFP-Nme9. **B.** A similar optical section through the MCC cytoplasm shows near-perfect colocalization of GFP-Nme9 with the ODA subunit RFP-Dnai2 in DynAPs. Dashed box indicates area shown at higher magnification in the inset. **C.** GFP-Nme9 only partially co-localizes with Dnaaf2-RFP. **D.** *En face* optical section just below the MCC apical surface reveals Wdr18-GFP localization near basal bodies labeled with RFP-centrin4. **E.** A similar section through the cytoplasm shows colocalization of GFP-Wdr18 with Dnaaf2-RFP in DynAPs. **F.** GFP-sf3a3 co-localizes with Dnaaf2-RFP. Scale bars = 10 μm.

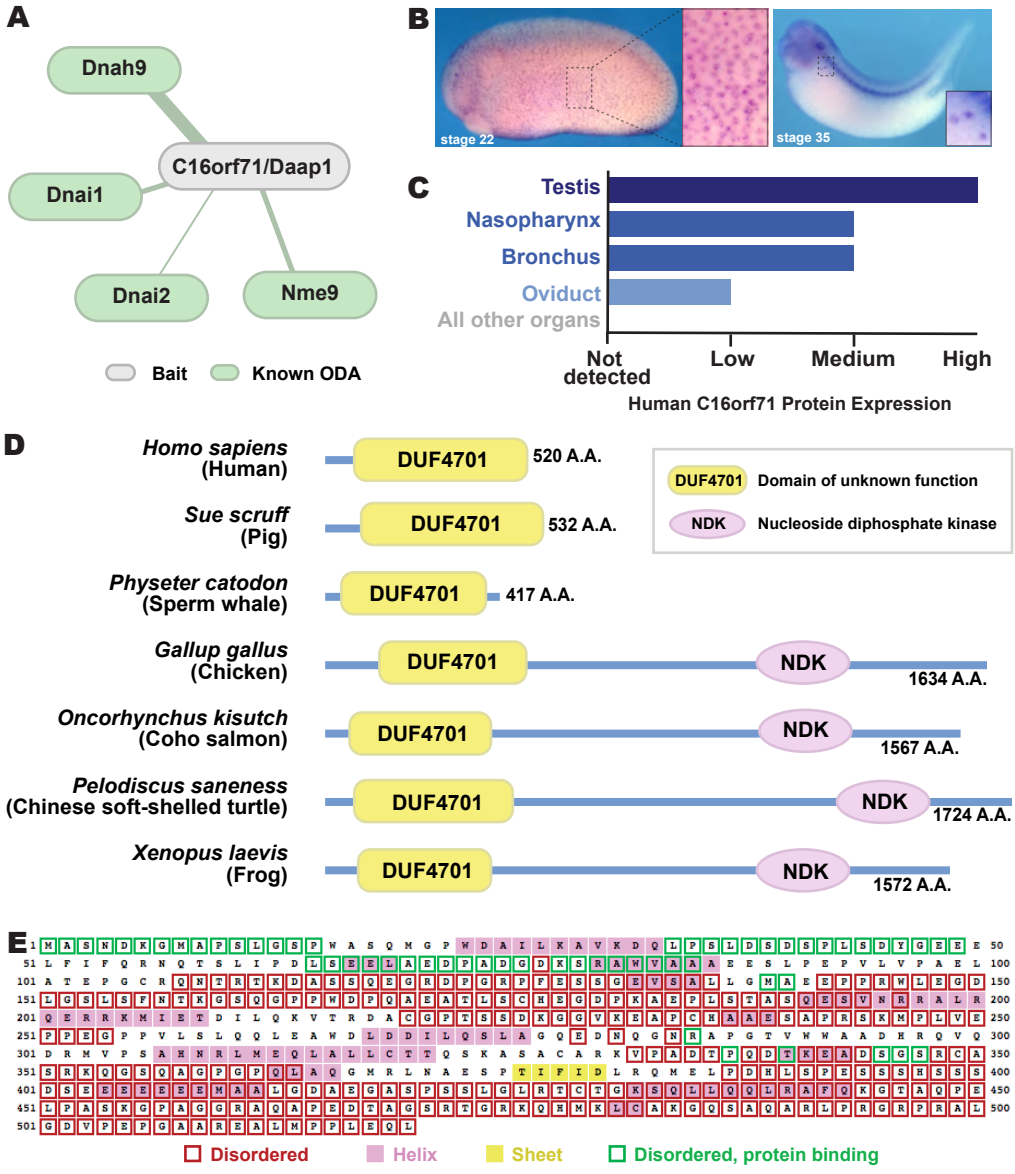

Lee et al., Figure 5

Figure 5. C16orf71/Daap1 is a novel ODA interactor specifically expressed in MCCs. **A.** Spoke diagram displaying C16orf71/Daap1 interactors; line weight indicates Log2 fold change of PSMs. **B.** *In situ* hybridization of *Daap1* in *Xenopus* reveals expression in epidermal MCCs (left) and MCCs in the nephrostomes (right). **C.** Graph showing C16orf71 protein expression levels in human tissues from the Human Protein Atlas (Uhlén et al., 2015). **D**. Domain organization of C16orf71/Daap1 orthologs across vertebrates from NCBI Orthologs. **E.** Domain prediction with human C16ORF71/DAAP1 sequence from the PSIPRED Protein Analysis Workbench for disorder and secondary structure prediction.

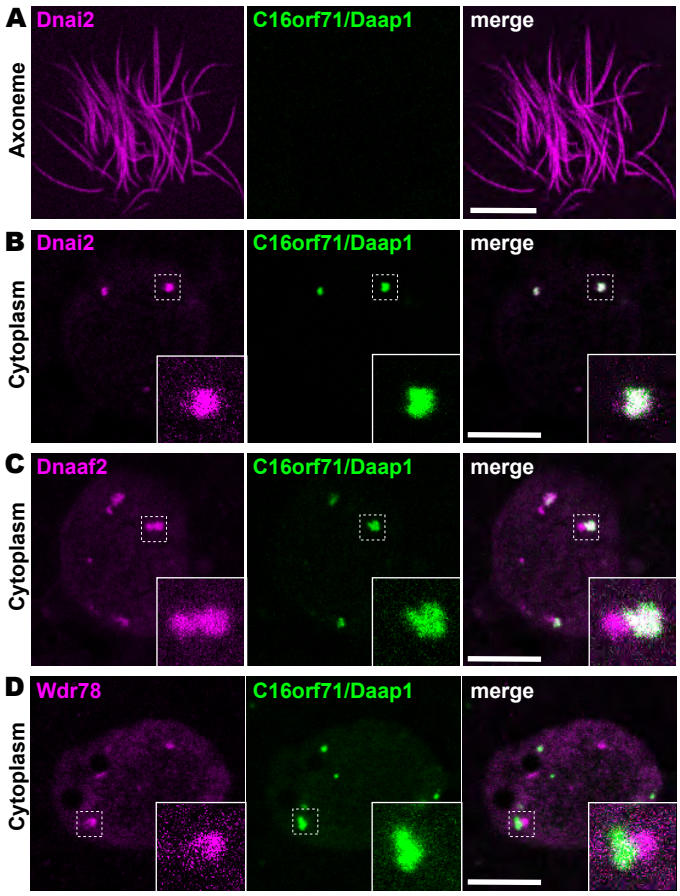

Lee et al., Figure 6

Figure 6. Daap1 is a DynAP-specific protein in *Xenopus* MCCs.
A. *En face* optical section above the apical surface of a *Xenopus* MCC reveals absence of Daap1-GFP in axonemes. **B.** A similar optical section through the MCC cytoplasm shows near-perfect colocalization of GFP-Daap1 with the ODA subunit RFP-Dnai2 in DynAPs. Inset shows higher magnification view of dashed box for each panel. **C.** GFP-Daap1 only partially co-localizes with Dnaaf2-RFP. **D.** GFP-Daap1 co-localizes only very weakly with the IDA subunit Wdr78-RFP.

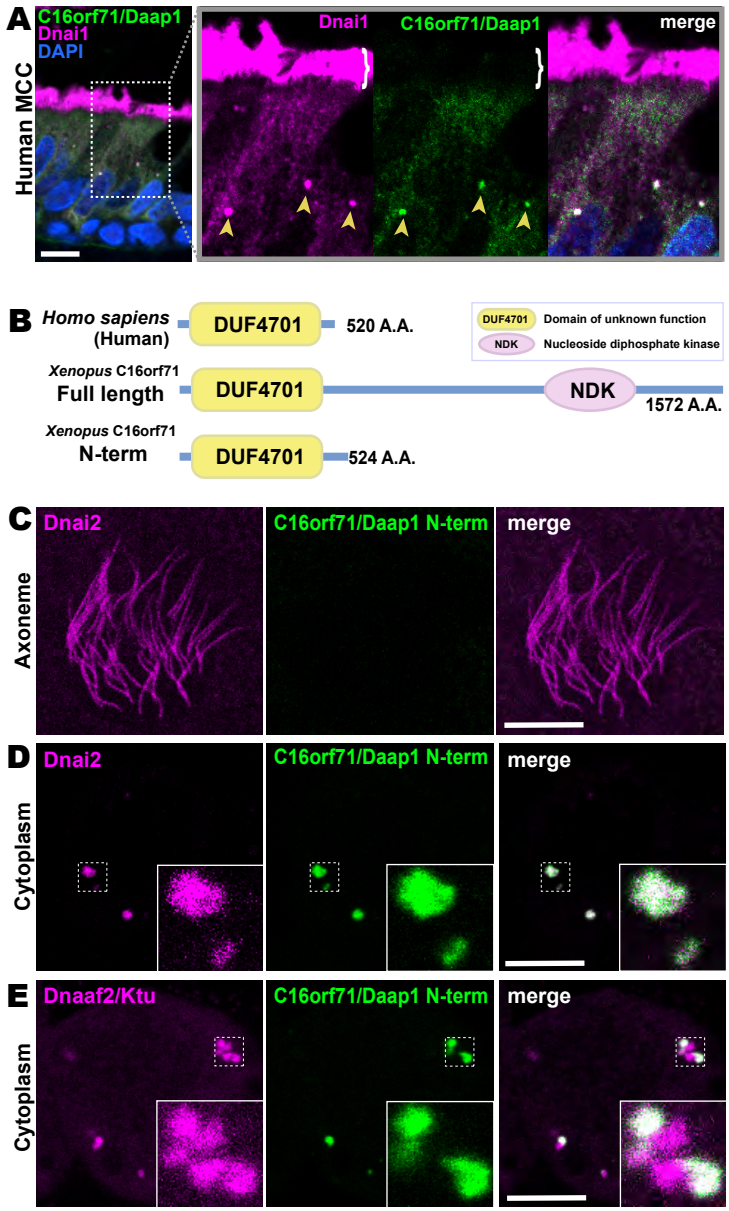

Lee et al., Figure 7

Figure 7. Human Daap1 is a DynAP-specific protein.
A. A primary human lung section immunostained for human Daap1 (green) and the ODA subunit DNAI1 (magenta). Boxed area indicates magnified region shown at right. Dnai1 strongly labels MCC axonemes (bracket) and also DynAPs in the cytoplasm (arrowheads). As in *Xenopus*, human Daap1 is not present in axonemes but is strongly enriched in DynAPs. (DAPI (blue) marks nuclei; scale bars = 10 μm.) **B.** Schematic of C16orf71 constructs: Xenopus Daap1-Nterm is truncated, containing only the DUF4701 domain, similar to human Daap1. **C.** *En face* optical section above the apical surface of a *Xenopus* MCC reveals absence of Daap1-Nterm-GFP in axonemes. **D, E.** Similar optical sections through the cytoplasm shows near-perfect colocalization of GFP-Daap1-Nterm with the ODA subunit RFP-Dnai2 and only partial co-localization with Dnaaf2/Ktu. In all cases, inset shows higher magnification view of dashed box for accompanying panels.

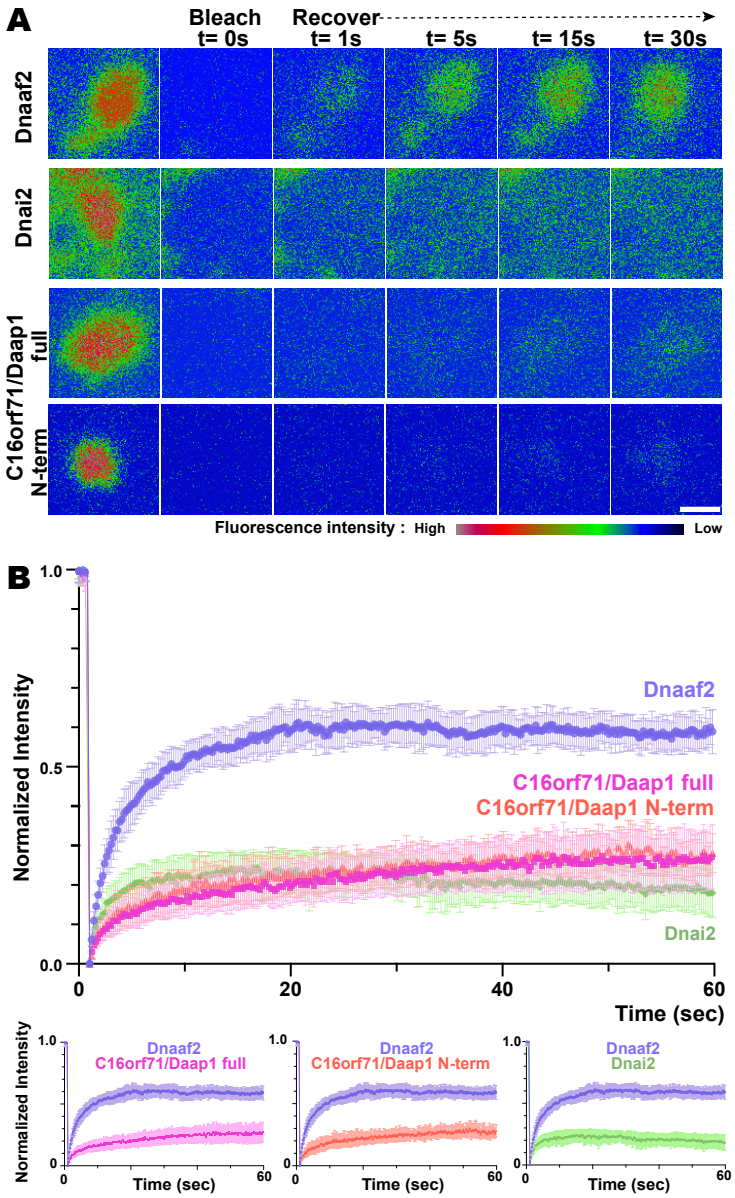

Lee et al., Figure 8

Figure 8. Daap1 is stably retained in DynAPs.
A. Stills from time-lapse imaging of FRAP for the assembly factor GFP-Dnaaf2, the ODA subunit GFP-Dnai2, GFP-Daap1 and GFP-Daap1-Nterm. Images are color-coded to highlight changes in pixel intensity (see key below images). **B**. Graphs displaying FRAP curves for GFP-Dnaaf2 (n=14), GFP-Dnai2 (n=12) GFP-Daap1 (n=26), and GFP-Daap1-Nterm (n=22).

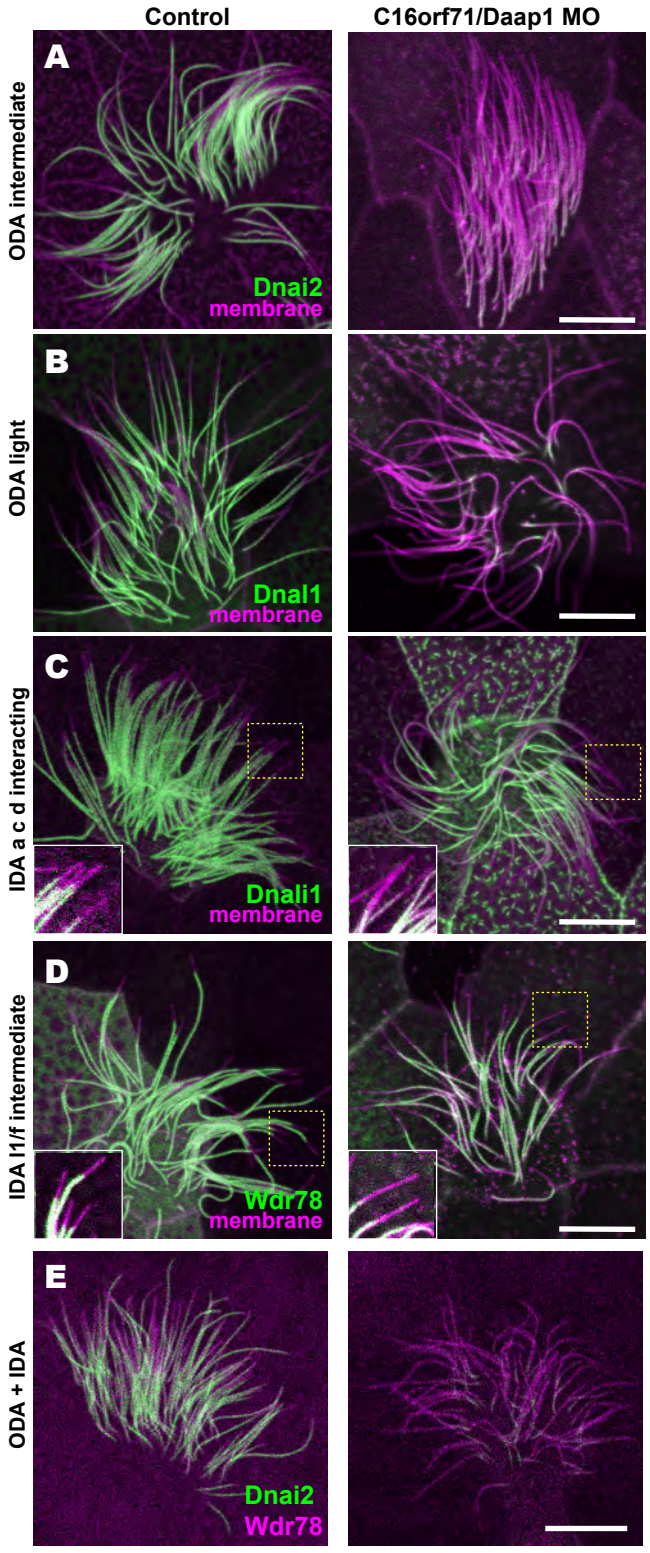

Lee et al., Figure 9

Figure 9. Loss of C16orf71 disrupts deployment of dynein subunits to the axoneme. **A-D**. *Xenopus* MCC axonemes labelled by membrane RFP (magenta) together with the GFP fusions to the indicated dynein subunits. Left panels are controls and right panels are Daap1 morphants. Both of Dnai2, an ODA Intermediated chain (A) and Dnal1, an ODA light chain (B) are severely reduced in the axoneme in C16orf71 morphants, while IDA subunits display only mild loss from the distal most axoneme (inset). Yellow boxes indicate regions shown in accompanying insets for each panel. **E**. MCCs co-expressing a marker for both ODAs (Dnai2, green) and IDAs (Wdr78, magenta). Loss of C16orf71 results in specific loss of ODAs in the axoneme. Scale bars = 10 μm.

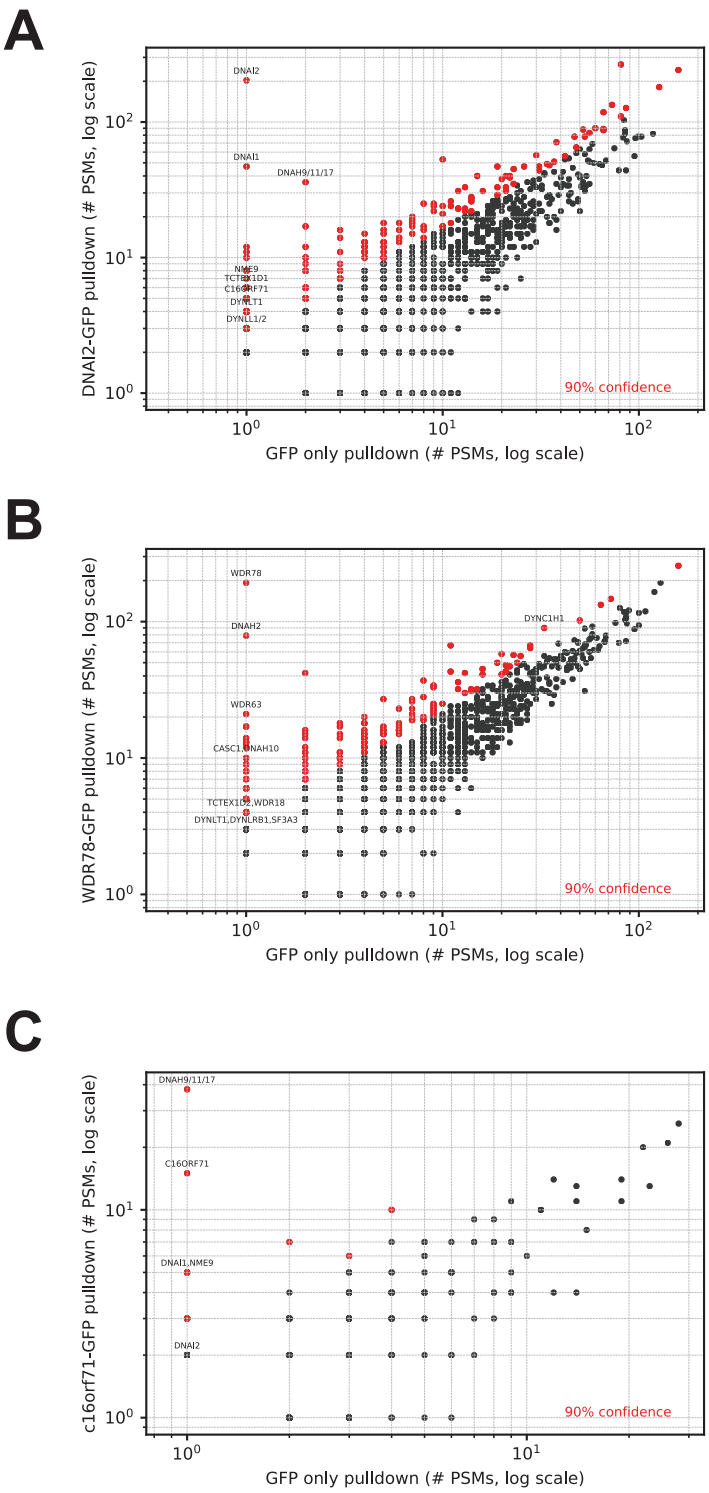

Lee et al., Supp Fig 1

Supp. Figure 1. Proteins co-precipitating with Wdr78, Dnai2, and C16orf71 by APMS. Interaction partners of (A) Dnai2, (B) Wdr78, and (C) C16orf71 were identified based on their enrichment in APMS of the GFP-tagged bait proteins (vertical axes) relative to APMS of the untagged GFP controls (horizontal axes). Confidence values were calculated by one-sided Z-test (see Methods). A pseudocount of 1 PSM was added to each protein for visualization on a log-log plot.

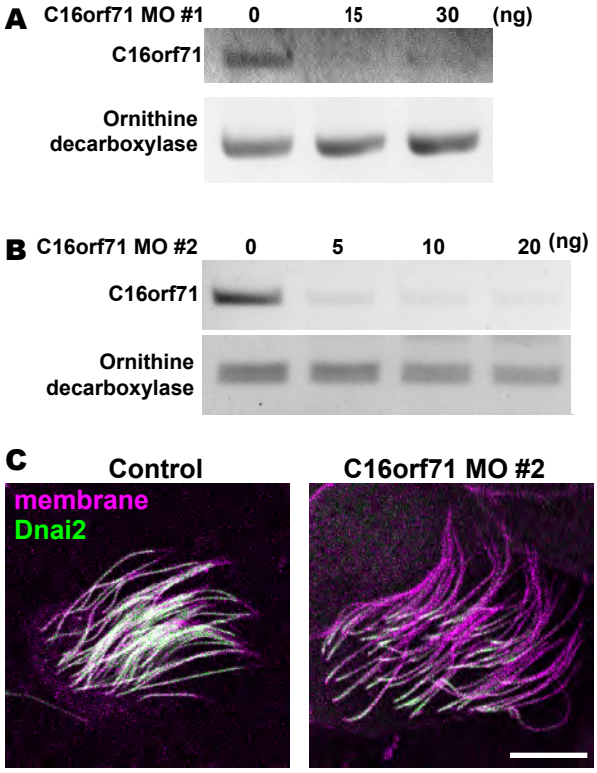

Lee et al., Supp Fig 2

Supp. Figure 2. Verification of C16orf71 morpholinos.
A-B. RT-PCR shows effective disruption of splicing by injection of C16orf71 MO #1(A) and #2 (B). Ornithine decarboxylase (ODC) was used as a loading control for the RT-PCR. **C.** Apical surface views labelled by membrane RFP (magenta) and GFP-Dnai2(green). Loss of C16orf71 by MO #2 results in reduction of Dnai2 in the axoneme, while GFP-Dnai2 reveals normal localization in control. Scale bar = 10 μm.

Supp. Tables 1-3. Tables showing orthogroups and proteins with PSMs identified by APMS with Dnai2, Wdr78, and C17orf71, respectively.